Clim. Past, 18, 975–988, 2022
https://doi.org/10.5194/cp-18-975-2022

Climate of the Past
Open Access
EGU

Humidity changes and possible forcing mechanisms over the last millennium in arid Central Asia

Shengnan Feng[1], Xingqi Liu[1], Feng Shi[2,3,4], Xin Mao[1,5], Yun Li[6], and Jiaping Wang[1]

[1]College of Resource, Environment and Tourism, Capital Normal University, Beijing 100048, China
[2]Key Laboratory of Cenozoic Geology and Environment, Institute of Geology and Geophysics, Chinese Academy of Sciences, Beijing 100029, China
[3]Georges Lemaître Centre for Earth and Climate Research, Earth and Life Institute, Université Catholique de Louvain, Louvain-la-Neuve 1348, Belgium
[4]CAS Center for Excellence in Life and Paleoenvironment, Beijing 100044, China
[5]Institute of Hydrogeology and Environmental Geology, Chinese Academy of Geological Sciences, Shijiazhuang 050061, China
[6]Qinghai Institute of Salt Lakes, Chinese Academy of Sciences, Xining 810008, China

Correspondence: Xingqi Liu (xqliu@cnu.edu.cn)

Received: 11 October 2021 – Discussion started: 22 October 2021
Accepted: 11 April 2022 – Published: 6 May 2022

Abstract. Hydroclimate changes have exerted a significant influence on the historical trajectory of ancient civilizations in arid Central Asia where the central routes of the Silk Road have been hosted. However, the climate changes on different timescales and their possible forcing mechanisms over the last millennium remain unclear due to low-resolution records. Here, we provide a continuous high-resolution humidity history in arid Central Asia over the past millennium based on the ∼ 1.8-year high-resolution multiproxy records with good chronological control from Lake Dalongchi in the central Tian Shan. Generally, the climate was dry during the Medieval Warm Period (MWP) and Current Warm Period (CWP) and wet during the Little Ice Age (LIA), which could be attributed to the influence of the North Atlantic Oscillation (NAO) and the Atlantic Multidecadal Oscillation (AMO). Furthermore, we find that the humidity oscillation was dramatic and unstable at multidecadal to century scales. Especially within the LIA, four wet episodes and three dry periods occurred. The continuous wavelet analysis and wavelet coherence show that the humidity oscillation is modulated by the Gleissberg cycle at the century scale and by the quasi-regular period of El Niño–Southern Oscillation (ENSO) at the multidecadal scale. Our findings suggest that the effect of the solar cycle and the quasi-regular period of ENSO should be seriously evaluated for hydroclimate predictions and climate simulations in arid Central Asia in the future.

1 Introduction

Arid Central Asia (ACA), far away from the ocean, is not only one of the driest and largest inland regions worldwide, but also the birthplace of the far-reaching ancient civilizations that spread along the Silk Road (Li et al., 2016; Narisma et al., 2007). Scarce precipitation, intense evaporation, and fragile ecosystems render this region sensitive to abrupt changes in effective humidity. Arid Central Asia is primarily controlled by the prevailing westerlies (F. Chen et al., 2019; Aizen et al., 2001; Sorrel et al., 2021; Huang et al., 2015b, 2014; Lauterbach et al., 2014). The moisture vapor was predominantly transported via the westerlies and originated from the North Atlantic Ocean, Mediterranean, Black Sea, and Aral–Caspian Sea (Lan et al., 2018; Chen et al., 2010; Huang et al., 2015b; Aizen et al., 2001; Mathis et al., 2014). Proxy records from ACA are valuable for understanding the driving factors and processes of underlying hydroclimate evolution in the inland region, which provides useful reference for human adaptation to hydroclimate changes at present and into the future (Li et al., 2016). On the sub-orbital scale, solar radiation controlled the intensity of the westerlies

through the variation of the meridional radiation gradient between high and middle latitudes, thus having the dominant influence on moisture changes of ACA during the Holocene (F. Chen et al., 2019; Jin et al., 2011). In addition, the suborbital-scale hydroclimate changes are also related to the shift of the Subtropical High, the strength and position of the Siberian High, North Atlantic Oscillation (NAO) mode, and the changes of the Laurentide and Scandinavian Ice Sheets (Sorrel et al., 2021; F. Chen et al., 2019; Carlson and Clark, 2012; Aichner et al., 2015; Wolff et al., 2016; Huang et al., 2014; Schwarz et al., 2017; Lauterbach et al., 2014).

In the past decades, a couple of proxy archives from ACA have been recorded the hydroclimate changes during the key periods such as the Medieval Warm Period (MWP) and Little Ice Age (LIA) over the past millennium (Ling et al., 2018; He et al., 2013; Lan et al., 2019; Song et al., 2015; Ma et al., 2008; Zhang et al., 2009; Rousseau et al., 2020; Chen et al., 2006; J. Chen et al., 2019). In earlier studies, a humid climate during the MWP and a dry climate condition during the LIA was documented by the tree ring of *Sabina przewalskii* (Kom.) (Zhang et al., 2003). This climate pattern was further demonstrated by the records from Lake Lop Nur and Daxigou profile on the northern slope of the central Tian Shan (Zhang et al., 2009; Ma et al., 2008). However, a growing body of studies based on the lacustrine sediments, ice cores, tree ring, and peat profiles show a generally similar climate pattern of a relatively dry MWP and a wet LIA in ACA over the last millennium (Chen et al., 2015, 2010; F. Chen et al., 2019; J. Chen et al., 2019; Lei et al., 2014; Rousseau et al., 2020; Lan et al., 2019; He et al., 2013; Song et al., 2015). Furthermore, there is some debate regarding the driving mechanism of the natural hydroclimate evolution over the last millennium. Many studies emphasize that internal climate variability (i.e., major sea and atmospheric modes) is supposed to be more marked than external factors (e.g., solar forcing) in influencing hydroclimate changes (F. Chen et al., 2019; Chen et al., 2006; Lan et al., 2019). According to this theory, the NAO and Atlantic Multidecadal Oscillation (AMO) play important roles by controlling the strength and shift of the westerly jet stream in determining hydroclimatic changes in ACA (Chen et al., 2015, 2010; Aichner et al., 2015; Lan et al., 2018, 2019). The El Niño–Southern Oscillation (ENSO) also contributes the climate variability in ACA on a multi-centennial timescale (Chen et al., 2015; F. Chen et al., 2019). In contrast, several paleoclimate records prefer to highlight the possible solar forcing to the humidity oscillation over the last millennium (Song et al., 2015; Zhao et al., 2009; He et al., 2013; Ling et al., 2018). For example, the solar imprint on the effective humidity fluctuations in ACA was proved by wavelet spectral analysis of the sediment record from Lake Manas (Song et al., 2015). Also, the $\sim$ 200-year moisture oscillations are related to the solar forcing recorded by the lake-level changes during the past 1000 years from Lake Hurleg (Zhao et al., 2009). Therefore, the climate changes on different time scales and their possible forcing mechanisms over the last millennium remain controversial. These controversies are largely attributed to low-resolution records or chronological uncertainties due to the old carbon effect (Chen et al., 2010; Q. Zhang et al., 2021), which limit our understanding of the hydroclimate evolution on decadal to centennial scales and of the relative role of external and internal drivers over the past millennium. More well-dated, high-resolution records are needed to further investigate the humidity evolution.

Here, we present a continuous $\sim$ 1.8-year high-resolution humidity reconstruction with good chronological control from Lake Dalongchi in the central Tian Shan of ACA over the past millennium (1180–2018 CE). Low- and high-frequency signals recovered from our reconstruction offer the potential to detect climate fluctuations at decadal to centennial scales, as well as long-term changes. Then, we explore the contribution of internal climate variability (which mainly refers to the NAO, AMO, and ENSO in this study) and solar activity to humidity oscillations on different timescales over the past millennium.

2 Study site

Lake Dalongchi (42°26′31″–42°26′58″ N, 83°16′48″–83°18′15″ E, 2400 m above sea level), located on the south slope of the central Tian Shan, is an ideal location for investigating hydroclimate changes in ACA (Fig. 1a), as the lake sits in the core area of the "westerlies dominated climatic regime (WDCR)" (F. Chen et al., 2019). The bedrock in the catchment of Lake Dalongchi is composed of pillow lava, gabbro, and limestone blocks included in a matrix of sheared calcareous turbidites. The ophiolitic mélanges are juxtaposed against Paleozoic sedimentary rocks, gneissic granitoids, and andalusite cordierite-bearing micaschist (Xiao et al., 2013; Ma et al., 2006; Gao et al., 1998). The main aquifer is hosted by ophiolitic rocks and categorized as a fissured rock aquifer (http://gis.geoscience.cn/website/hg/viewer.htm, last access: 8 January 2022). This aquifer has multi-scale hydraulic discontinuities and low groundwater potentiality due to the structural heterogeneities of the ophiolitic rocks (Lods et al., 2020; Jeanpert et al., 2019; Boroninaa et al., 2003).

Lake Dalongchi is a small alpine freshwater lake formed by glacial moraine damming and has a mean pH of 8.03 and a salinity of 0.31 g L^{-1}. Both the north and south sides of the lake are surrounded by steep mountains (Fig. 1b). The lake is mainly fed by the river originating from mountains on the east, precipitation within the catchment, and glacial meltwater from the surrounding mountains at high elevations. The lake water flows out into Lake Xiaolongchi through a tunnel under the moraine and the outflow discharge is low. Then the lake water from Xiaolongchi flows westwards into the Kuche River basin (Fig. 1b).

Measured in July 2018, the lake covers a surface area of $\sim$ 1.4 km^2 and has a catchment area of $\sim$ 131 km^2. The max-

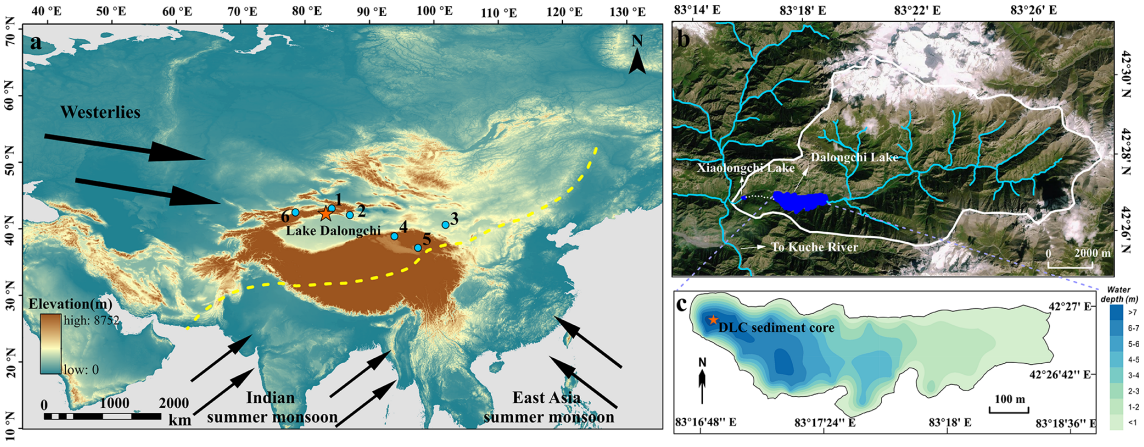

Figure 1. Maps of the study site. **(a)** Locations of Lake Dalongchi and other humidity records in arid Central Asia, mentioned in the text. Sites 1–6 denote the Bayanbuluk meteorological station, Lake Bosten (Chen et al., 2006), Badian Jaran Desert (Ma and Edmunds, 2006; Gates et al., 2008), Lake Sugan (He et al., 2013), Lake Gahai (He et al., 2013), and Lake Ala Kol (Rousseau et al., 2020), respectively. The dashed yellow line indicates the boundary of the modern Asian summer monsoon; the mid-latitude inland region on the western side of the modern Asia summer monsoon boundary line is arid central Asia (ACA) (Chen et al., 2010; F. Chen et al., 2019). The map was generated using ArcMap 10.2 software (ESRI, USA, http://www.esri.com, last access: 9 February 2020). **(b)** Watershed map of the study site. **(c)** Bathymetric contour map of Lake Dalongchi with the coring site.

imum water depth of Lake Dalongchi reaches 7.4 m in the western lake, and its depth largely decreases from west to east (Fig. 1c). Alpine coniferous forests dominated by Picea primarily thrive on the southern and western slopes of the surrounding mountains, while the northern slope is covered by herbs such as Chenopodiaceae, *Artemisia*, Poaceae, and Cyperaceae. According to the records from 1958 to 2019 at Bayanbuluk Station which is located ∼ 100 km to the northeast of Lake Dalongchi, the mean annual temperature is −4.6 °C with a July average of 10.9 °C and a January average of −26.4 °C, and the mean annual precipitation and evaporation are 270 and 3200 mm, respectively. The mean annual precipitation is far less than the evaporation capacity. Moreover, most of the precipitation occurs as convective rainfall from June–August (Lan et al., 2018). The prevailing wind is from the northwest, and the annual average wind speed is only 2.73 m s^{-1}. The average number of sandstorm days is less than 5 d yr^{-1} based on the meteorological records from 1959 to 1998 (B. Zhang et al., 2021; Zhou et al., 2002).

3 Materials and methods

3.1 Sampling

In July 2018 and August 2019, we retrieved several parallel long sediment cores from Lake Dalongchi at a maximum water depth of 7.4 m using the UWITEC platform manufactured in Austria, and several short cores using a piston gravity corer (Fig. 1c). To determine overlaps and ensure the continuity of the cores, magnetic susceptibility (MS) nondestructive scanning of all long and short sediment cores was used to obtain a 6.95 m long composite core (DLC1819) (Fig. 2).

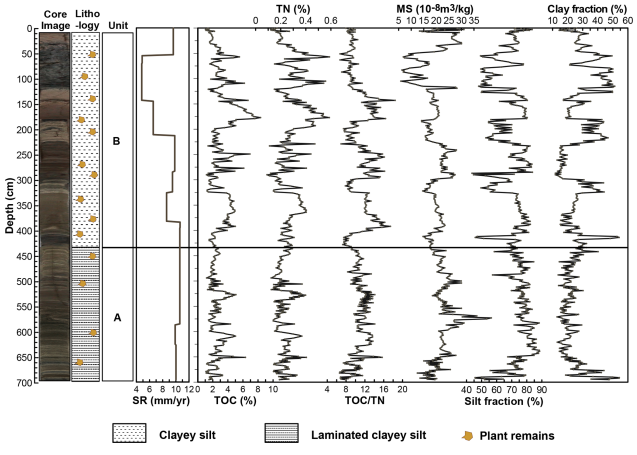

Figure 2. Sedimentary lithology and multi-proxy variation versus depth for the composite DLC1819 core.

3.2 Laboratory analysis

The DLC1819 core was subsampled at 1 cm intervals. All subsamples were stored in a freezer in our laboratory at a constant temperature of 4 °C and used for MS, grain size, total organic carbon (TOC), and total nitrogen (TN) analyses. Samples for MS were dried at below 40 °C in a constant temperature air-blast drying oven and ground and packed into standard plastic boxes with a capacity of 2·2·2 cm^3. A Bartington MS2 susceptibility meter was used to measure magnetic susceptibility. Samples used for grain size measurement were pretreated with 10–20 mL of 10 % H_2O_2 to remove organic matter and then with 10 mL of 10 % HCl to remove carbonates; next, samples were rinsed with deionized water and fi-

nally treated with 10 mL 0.05 M $(NaPO_3)_6$ on an ultrasonic vibrator for 10 min to promote dispersion. Grain size distributions were determined using Malvern/MS 3000 laser grain size analyzer. The samples used for TOC and TN determination were decalcified with 10 % HCl and rinsed repeatedly with deionized water. Then, ∼ 3–5 mg dried and ground samples were analyzed using the EURO EA 3000 elemental analyzer.

Terrestrial plant remains at different depths in the DLC1819 core were used for accelerator mass spectrometry (AMS) ^{14}C measurements at Beta Analytic Inc., U.S.A. (Table 1). The uppermost sediments were used for the radiometric dating by measuring the activity of ^{137}Cs as a function of depth. The samples of the uppermost sediments at 0.5 cm intervals were dried and ground to less than 100 mesh and then loaded into the 5 mL cylindrical PVC tube. Radio-activity of ^{137}Cs was measured using a spectrum analysis system consisting of a high-purity germanium well detector produced by EG& G Ortec Company (USA), Ortec 919 spectrum controller, and IBM microcomputer with a 16 K channel multichannel analyzer.

4 Results

4.1 Lithology and chronology

DLC1819 core is mainly composed of clayey silt and can be divided into two lithology units from bottom to top (Fig. 2). Unit A (695–430 cm) is mainly composed of dark or light brown clayey silt with clear lamination. Unit B (430–0 cm) has a dramatic lithological variation characterized by brown or greyish-green clayey silt without obvious lamination. There are lots of the plant residues in the core, but they are more abundant in Unit B than in Unit A (Fig. 2).

A significant increase in ^{137}Cs activities occurred at approximately 71 cm, which could be attributed to the onset of rising concentrations of ^{137}Cs in the Northern Hemisphere (NH) at 1952 CE (Fig. 3a). The distinct peak at the depth of 64 cm was taken as the 1963 CE global fallout maximum (Pennington et al., 1973) (Fig. 3a). We established the age–depth model of DLC1819 based on the 2 ^{137}Cs ages and nine radiocarbon ages by the Bacon 2.5.7 procedure in R software using the Bayesian method (Blaauw and Christen, 2011) (Fig. 3b). Chronology results show that the DLC1819 core covers the past 840 years with an approximate average sedimentation rate of 9.0 mm yr^{-1}. Unit A has unusually stable sediment accumulation rates with an average of 10.3 mm yr^{-1}, while the sediment accumulation rates vary greatly from 4.9 to 10.6 mm yr^{-1} in Unit B (Fig. 2).

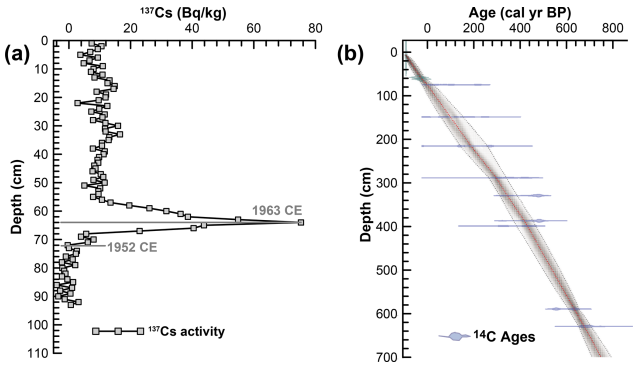

Figure 3. Age–depth model for the DLC1819 core of Lake Dalongchi. **(a)** The ^{137}Cs activity versus depth in the uppermost sediments. **(b)** Bayesian age-model for the calibrated ages. The black dotted lines indicate the 95 % probability intervals of the model.

4.2 TOC, TN, C/N, MS, grain size

TOC and TN results show broadly similar changes and vary between 1.14 % and 8.33 % and between 0.09 % and 0.59 %, respectively (Fig. 2). C/N ratios fluctuate between 7.95 and 18.42 with an average of 10.88, and the values of C/N ratios exceed 10 at the depths of 440–650 cm, 330–400 cm, 230–300 cm, and 130–180 cm (Fig. 2). MS values of the DLC1819 core vary between 5.90 and 41.89×10^{-8} m^3 Kg^{-1} with an average of 20.66×10^{-8} m^3 Kg^{-1} (Fig. 2). The silt percentage fluctuates from 43.64 % to 88.50 % with an average of 71.91 % while the variation of clay percentage has an opposite trend to that of silt, and its values vary from 11.84 % to 54.26 % with an average of 25.97 % (Fig. 2). Sand content only accounts for 2.43 % of the total grain size on average. Generally, the higher values of the MS and silt content and the lower clay content correspond to the higher C/N ratios and vice versa (Fig. 2).

5 Discussion

5.1 Proxy interpretation and humidity index reconstruction

The characteristics of 125–500 µm particles with well-developed surface structure can fully reflect the transport distance and dynamic conditions of sediment in a specific environment; short distances and weak transport dynamics usually result in a poor grain roundness of sediments (Moral Cardona et al., 2005; Mahaney et al., 2004). The surface microscopic properties of four randomly selected samples in the DLC1819 core show that the grains in the range of 125–500 µm are characterized by poor roundness with an angular outline which is quite different from the eolian materials (M. Zhang et al., 2021) (Fig. S1 in the Supplement), excluding the possibility that the clastic particles are derived from eolian deposition in Lake Dalongchi.

Table 1. Accelerator mass spectrometry (AMS) ^{14}C dating results of DLC1819 core.

No.	Lab. no	Sample ID	Composite depth (cm)	Analyzed material	δ^{13}C (‰)	^{14}C age/BP	Calendar age/CE
1	Beta – 514897	DLC-1-1-61	69	Wood	−24.9	90 ± 30	1870–1928
2	Beta – 507553	DLC-1-1-135	143	Wood	−27.4	170 ± 30	1721–1818
3	Beta – 507554	DLC-1-2-82	210	Wood	−31.4	230 ± 30	1635–1684
4	Beta – 507555	DLC-1-2-155	283	Wood	−26.1	340 ± 30	1470–1640
5	Beta – 507556	DLC-1-3-61	324	Wood	−28.1	430 ± 30	1420–1498
6	Beta – 507557	DLC-1-3-119	382	Wood	−22.3	440 ± 30	1416–1490
7	Beta – 514898	DLC-1-3-131	394	Wood	−23.7	370 ± 30	1446–1528
8	Beta – 514901	DLC-3-5'-37	585	Wood	−23.6	670 ± 30	1274–1320
9	Beta – 542591	DLC2019-1-5-76	625	Wood	−23.1	800 ± 30	1184–1275

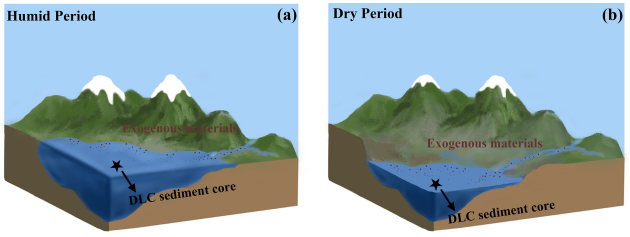

Figure 4. Schematic diagram illustrating a simple explanation of the lacustrine depositional process in the Lake Dalongchi region. Lake level condition and the transport process of exogenous materials in the humid period **(a)** and the dry period **(b)**.

Terrestrial plants usually have C/N ratios of more than 20 (Meyers, 1994, 2003), so the increased C/N ratios in Lake Dalongchi sediments reflect the input amount of allochthonous organic matter (Fig. 2). Synchronously, the increase in the MS values and silt content also indicates the increased input of detrital materials and the intensified erosion of the basin (Fig. 2). Given that the weak inflows of the runoff into Lake Dalongchi, which is a shallow and a small lake with an area only of 1.4 km^2, the distance from the lakeshore to the sampling site is the key to determining the amount of exogenous detrital materials in the core. Therefore, during the humid (dry) period represented by high (low) lake level and enlarged (reduced) lake area, exogenous materials containing magnetic minerals, coarse grain components, and terrestrial plants were poorly (easily) transported to the sampling site due to the long (short) distance from the lakeshore and reduction (intensified) erosion in the basin (Fig. 4). Thus, the high MS values, silt content, and C/N ratios indicate a dry climate and vice versa (Fig. 4).

Accordingly, multiple proxies, such as C/N ratios, MS, silt, and clay fractions, were synthetically employed to reconstruct the humidity index (HI) in the Lake Dalongchi region over the past millennium (Fig. 5). As the high values of C/N ratios, MS, and silt contents and low values of clay content reflect the arid climatic environment, the first three records multiplied by −1 and clay content were normalized

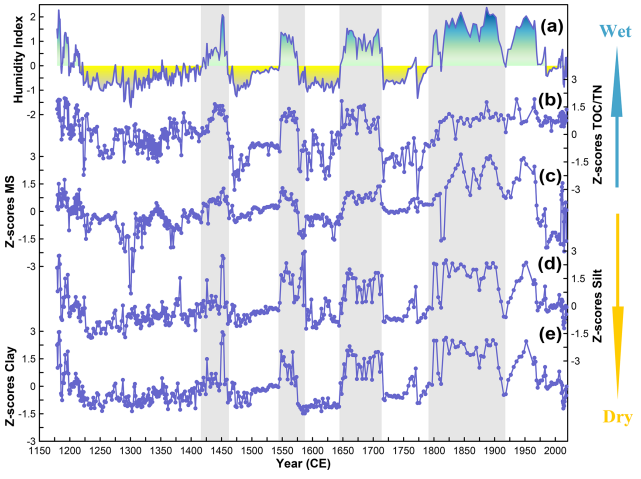

Figure 5. Humidity index reconstruction **(a)** based on the Z scores of total organic carbon / total nitrogen (TOC/TN) ratios **(b)**, the Z scores of magnetic susceptibility (MS) **(c)**, the Z scores of silt fraction **(d)**, and the Z scores of clay fraction variation **(e)** in the DLC1819 core in Lake Dalongchi. Light grey bars highlight intervals of increased humidity in Lake Dalongchi during the LIA.

to a Z score (Fig. 5b, c, d, e). Then the HI was derived from the average of the normalized standard Z scores. Positive and negative Z scores indicate wet and dry climatic conditions (Fig. 5a).

5.2 Humidity changes over the last millennium

There is a generally positive correlation ($r = 0.298*$) between the reconstructed HI and the instrumental relative humidity records over the past 60 years from the nearby Bayanbuluk meteorological station at the 0.05 significance level, verifying the reliability of the humidity reconstruction (Fig. 6a). The HI changes show that the climate was dry during the MWP (1180–1420 CE) and CWP (1920–2018 CE) and wet during the LIA (1420–1920 CE) (Fig. 6b). Moreover, our preliminary palynological data also show a dry climate characterized by herb pollen (∼ 71 %) dominated by

Artemisia, Chenopodiaceae, and Poaceae during the MWP and a wet climate characterized by the rapid increased tree pollen dominated by *Picea* (up to 45 %) during the LIA (unpublished data). This multi-centennial climate pattern is generally in agreement with the hydroclimatic patterns revealed by recent numerous studies in ACA (Chen et al., 2006; Song et al., 2015; Lan et al., 2018, 2019; Zhao et al., 2009; He et al., 2013; Ma and Edmunds, 2006; Gates et al., 2008; Rousseau et al., 2020) (Fig. 6c, d, e, f, g, h), although several studies tend to suggest humid climate conditions during the MWP in ACA (Zhang et al., 2009; Ma et al., 2008; Zhang et al., 2003). A total 5 of the 17 records selected on the basis of reliable chronologies and robust proxies from ACA show a relatively dry MWP, and a wet LIA characterized not only by relatively humid but also by high precipitation (Chen et al., 2010) (Fig. 6c). Recently, records from Lake Ala Kol, Kyrgyzstan, reveal the cold and wet climate conditions during the LIA indicated by the prominent glacier advances (Rousseau et al., 2020) (Fig. 6h), which corresponds to the maximal ice accumulation in the Guliya ice core (Rousseau et al., 2020; Yang et al., 2009). Thus, the humidity changes of Dalongchi lake do not indicate a local signal but a regional signal, i.e., the typical "westerlies-dominated climatic regime" (WDCR) (F. Chen et al., 2019).

The previous study shows that the higher anomalous climatic instability during the LIA compared to the MWP, suggesting the moisture instability prefers to occur within the conditions of an overall cold climate (J. Chen et al., 2019). However, it is not clear how the specific unstable wet and dry climate fluctuated during the LIA, due to the relatively low-resolution records in ACA (Chen et al., 2006; Zhao et al., 2009; Lan et al., 2019). The HI reconstruction of Lake Dalongchi provides new evidence for the unstable hydroclimatic variability during the LIA (Fig. 6b). Four wet episodes with the sharp high HI values were recorded for 1420–1470, 1550–1600, 1650–1720, and 1800–1920 CE, and three dramatic dry periods with the low HI values were recorded for 1470–1550, 1600–1650, and 1720–1800 CE during the LIA (Fig. 6b). Our high-resolution reconstruction clearly documented several obvious and dramatic secondary humidity fluctuations within the LIA, which are not clearly captured in other current records from ACA (Chen et al., 2006; Ma and Edmunds, 2006; Gates et al., 2008; He et al., 2013) (Fig. 6). The climatic instability during the LIA can also be reflected by the dramatic lithological variations and the unstable sediment accumulation rates in Unit B (Fig. 2). Moreover, continuous wavelet transform (CWT) of HI exhibits a significant century-scale dominant oscillation ranging from ~ 88 to 146 years, which is nearly throughout the entire time series and prominent in 1450–1800 CE, as well as a strong ~ 50- to 65-year multidecadal oscillation at a 95 % confidence level relative to the red noise spectrum (Fig. 7a).

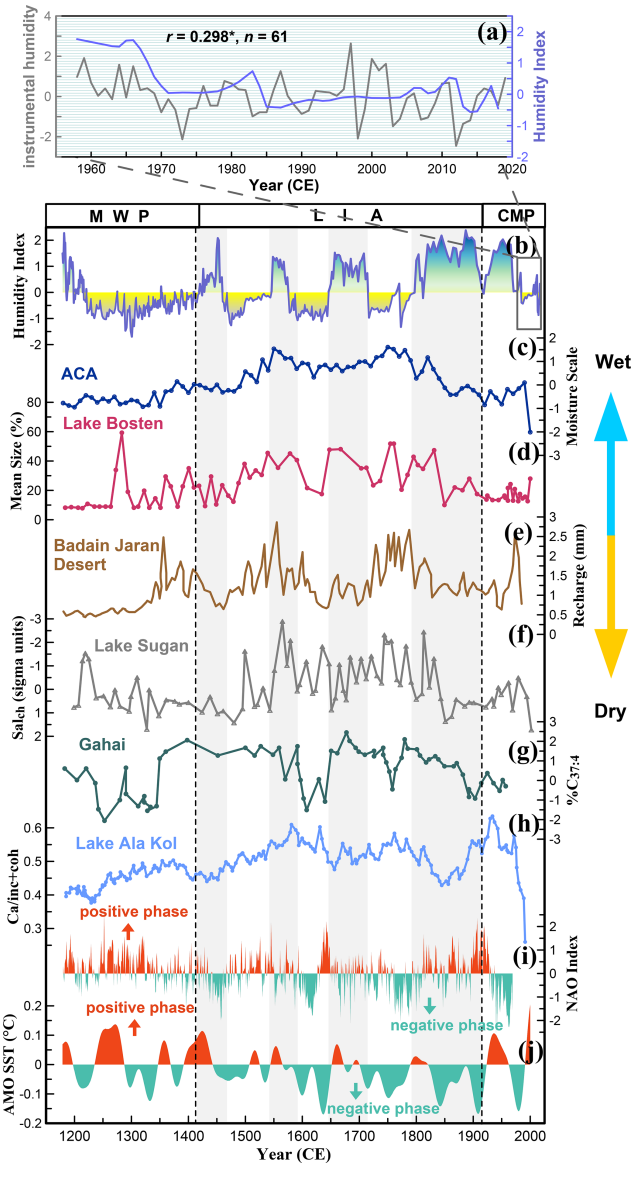

Figure 6. Humidity index (HI) of Lake Dalongchi and comparison to other records in ACA over the last millennium. **(a)** Comparison between the HI (blue line) and the standardized instrumental effective humidity recorded by Bayanbuluk meteorological station (grey line). An asterisk (*) represents the 0.05 significance level. **(b)** The reconstructed HI for the past millennium (1180–2018 CE). **(c)** The synthesized moisture curve over the last millennium in ACA (Chen et al., 2010). **(d)** Variations in the mean grain size along the BST04H core in Lake Bosten (Chen et al., 2006). **(e)** The unsaturated recharge history in Badian Jaran (Gates et al., 2008; Ma and Edmunds, 2006). **(f)** Chironomid inferred salinity (Salch) in SG03I of Sugan Lake (Chen et al., 2009). **(g)** $\%C_{37:4}$ from Lake Gahai (He et al., 2013). **(h)** Ca/inc + coh from Lake Ala Kol (Rousseau et al., 2020). **(i)** The reconstructed NAO (Ortega et al., 2015). **(j)** The reconstructed AMO (Wang et al., 2017). Light grey bars highlight intervals of increased humidity in Lake Dalongchi during the LIA.

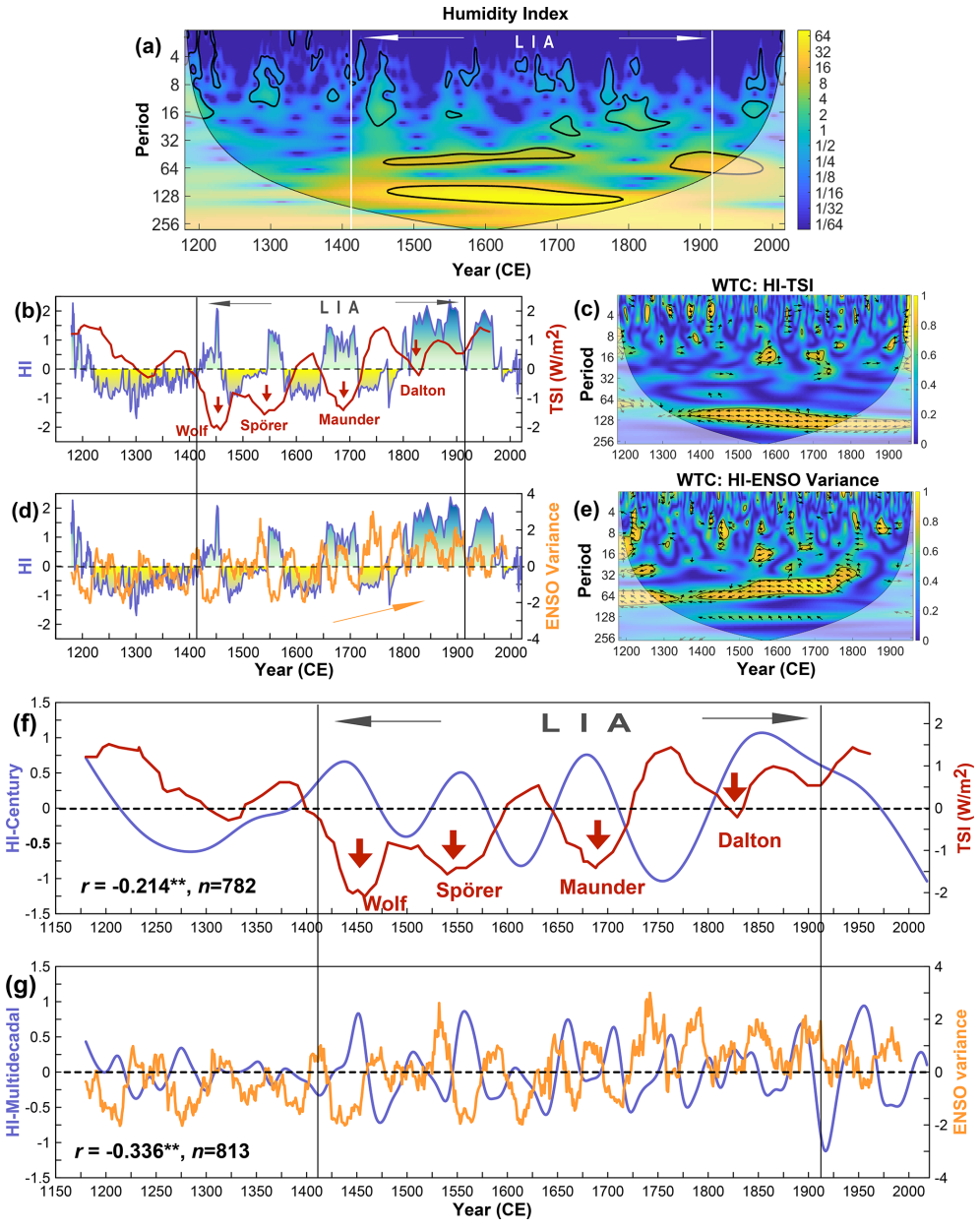

Figure 7. The wavelet analysis of the HI and the relationship between the HI and the TSI or ENSO. **(a)** Continuous wavelet (CWT) power spectrum of the HI. The irregular thick black contour represents the 95 % confidence level against red noise, and the thin curved black solid line is the cone of influence (COI) (Grinsted et al., 2004). **(b)** A comparison between the HI and the reconstructed total solar irradiance (TSI) (Bard et al., 2000). Wolf, Spörer, Maunder, and Dalton represent several grand solar minimums that occurred during the LIA. **(c)** The wavelet coherence (WTC) result between the HI and the TSI (Bard et al., 2000). **(d)** As **(b)**, but for ENSO variance reconstruction (Li et al., 2011). Orange arrows represent the enhanced ENSO amplitude trend. **(e)** As **(c)**, but for ENSO variance (Li et al., 2011). **(f)** A comparison between the century component of HI and TSI (Bard et al., 2000). **(g)** A comparison between the multidecadal component of the HI and ENSO variance reconstruction (Li et al., 2011). The 95 % confidence level against red noise is shown as an irregular thick black contour. The black arrows illustrate the relative phase relationship: arrows pointing right are in phase and those pointing left are anti-phase (Grinsted et al., 2004). Two asterisks (**) represent the 0.01 significance level.

5.3 Possible forcing mechanisms

5.3.1 The influence of NAO and AMO

Several studies have linked hydroclimate changes in arid Central Asia to the NAO and the AMO over the last millennium (Aichner et al., 2015; Yan et al., 2019; Chen et al., 2006; Lan et al., 2018; F. Chen et al., 2019; J. Chen et al., 2019). On multidecadal timescales, most records show that the NAO and AMO are dominated by alternating sea surface temperatures (SSTs) and sea-level pressure (SLP) anomalies, respectively (Ortega et al., 2015; Knudsen et al., 2014). The climatic instability during the LIA may be link to the NAO and AMO via the westerlies (J. Chen et al., 2019). However, the relationship between HI, NAO, and AMO is ambiguous on multidecadal timescales (Fig. 6b, i, g). Although the wavelet coherence (WTC) results show that the NAO and HI have approximately $\sim$ 25-, 50-, and 128 year periodicities, and the AMO and HI have the periodicities of $\sim$ 32, 70, and 128 years, these periodicities are nonpersistent (Fig. S2). Therefore, our results suggest that the periodic variations in NAO and AMO themselves have little influence on the humidity fluctuation in Lake Dalongchi at the multidecadal timescale.

However, on multi-centennial timescales, the dominant dry climate conditions during the MWP and humid climate conditions during the LIA seems related to the relatively positive and negative phases exhibited in the NAO and AMO, respectively (Fig. 6b, i, g). Previous studies indicate the negative phase of the NAO and AMO during the LIA favors increasing precipitation in ACA (J. Chen et al., 2019; Chen et al., 2015, 2006, 2016; Lan et al., 2018; Aichner et al., 2015). During the MWP, the positive phase of the NAO with enhanced pressure between the Azores High and the Icelandic Low would lead to strengthened zonal flow, and the axis of maximum moisture transport and preferred storm track extend to the north and east (Trouet et al., 2009). In contrast, the axis of maximum moisture transport and preferred storm track migrated southwards when the NAO was in a negative phase during the LIA (Hurrell, 1995). A general cold (warm) phase of the AMO corresponds to the negative (positive) NAO phase during the LIA (MWP) (Wang et al., 2017; Ortega et al., 2015), leading to a weaker (strong) upper-level jet stream intensity and further resulting in development (recession) of the through-ridge system, consequently contributing to the increased (decreased) precipitation in ACA (J. Chen et al., 2019). Thus, the multi-centennial behavior in our reconstruction might be related to the influence of the NAO and AMO on hydroclimate changes between the MWP and the LIA.

5.3.2 The role of the Gleissberg cycle

Solar forcing has been treated as a critical factor for influencing key components (e.g., temperature, precipitation, evaporation, winds, ocean circulation, and iceberg transport) of the climate system (Sha et al., 2016; Bond et al., 2001; Bard and Frank, 2006; Knudsen et al., 2014). As the largest dry inland regions on the globe, the climate records from ACA are valuable for investigating the fingerprint of solar forcing. We compared HI with the reconstructed total solar irradiance (TSI) (Bard et al., 2000) and found a strong link and inverse relationship between the HI and TSI, especially during the LIA (Fig. 7b). The HI increased significantly and reached its peak during the several grand solar minimums (Wolf, Spörer, Maunder, Dalton), whereas the humidity decreased rapidly in the maximum solar activity period (Fig. 7b). The WTC spectrum between HI and TSI shows a strong correlation and antiphase pattern (Fig. 7c). Periodicities of significant coherence for HI and TSI occurred at $\sim$ 88 to 146 years, particularly from 1400 CE to the present. Arrows in the significant coherence spectral area point almost entirely to the left, implying the persistent negative correlation of HI and TSI (Fig. 7c). Therefore, the WTC result confirms that the persistent $\sim$ 88–146-year cycle of HI in CWT is associated with solar activity (Fig. 7a, c). The cycle of 88–146 years should be attributed to the century-scale solar cycle of Gleissberg (Gleissberg, 1958, 1965; Ogurtsov et al., 2015) (Fig. 7a). Accordingly, we extracted this century signal from the original HI series based on the ensemble empirical mode decomposition (EEMD), a new noise-assisted data analysis (NADA) method (Wu and Huang, 2009; Huang et al., 1998). The relationship between the century component and TSI has an apparent correlation ($r = -0.217**$) and a clear coherence spectral area (Figs. 7f and S3a). The HI shows an extreme instability accompanied by obvious secondary oscillations of cold–wet and warm–dry at century timescales during the LIA under the regulation of solar activity (Fig. 7f). This verifies the critical role of the Gleissberg solar cycle in controlling the effective humidity at the century scale during the last millennium in ACA. Shindell et al. examined the climate response to the solar forcing at the Maunder minimum and indicated that even relatively little solar activity might play a primary role in century-scale climate change in NH (Shindell et al., 2001). The possible solar contribution of the Gleissberg century cycle to climate changes over at least the last millennium has been reported from the North Atlantic region (Moffa-Sánchez et al., 2014; Ogurtsov et al., 2002a, b, 2015). In arid Central Asia, several records documented the solar fingerprint by the evidence of $\sim$ 200-year periodicity between the proxy data and solar activity time series (Zhao et al., 2009; Yin et al., 2016), and sediment records from Lake Toson and Lake Manas exhibited periodicities of 93 years and 70 to 100 years respectively through the spectral and wavelet analysis, which may be linked with the Gleissberg solar cycle (Ling et al., 2018; Song et al., 2015). However, still, rare records in ACA documented the good relationship between the effective humidity changes and the fluctuations of the Gleissberg cycle. Our reconstruction provides strong evidence for negative link between the Gleissberg solar cycle and humidity changes at century timescales during the last millennium in ACA.

The confusion we focus on now is how solar activity significantly affected hydroclimate fluctuations in ACA over the last millennium. Several studies proposed that the solar forcing may influence the variability of the sea–atmospheric modes, the NAO in particular (Swingedouw et al., 2011; Kirov and Georgieva, 2002; Kodera, 2002; Gimeno et al., 2003). Kodera (2002) suggests that the NAO extends to the stratosphere during the high solar activity and to the troposphere during the low solar activity. Such a relationship between the solar activity and troposphere or stratosphere subsequently determines the positive or negative phase of NAO (Shindell et al., 2001; Kodera and Kuroda, 2002; Gray, 2003). Solar irradiance also has been served as a trigger for the shifts of the precipitation-bearing westerlies during winter (Brahim et al., 2018; Kodera, 2002; Yukimoto et al., 2017). Ultimately, the solar variability indirectly affects the hydroclimate changes through modulating the NAO state, suggesting solar regulation for hydroclimate might be amplified on a regional scale through atmospheric circulation (Ineson et al., 2011; Shindell et al., 2001; Gray, 2003; Brahim et al., 2018; Kodera, 2002; Yukimoto et al., 2017).

However, for ACA far from the ocean with scarce precipitation and intense evaporation, the mechanism of solar forcing on humidity may be direct. Our reconstruction reveals the robust negative relationship between the TSI and HI, but the ambiguous relationship between the NAO and HI (Figs. 6, 7). The paleoclimate records from ACA also highlight that the intense evaporation and direct heating caused by the enhanced solar irradiance control the effective humidity (Liu et al., 2019; Song et al., 2015; He et al., 2013; Wu et al., 2020; Ling et al., 2018; Zhao et al., 2009). To further investigate the potential feedback processes between the solar variability and effective humidity at century timescales in ACA, we performed a transient experiment forced only by the TSI for the last millennium using the Max Planck Institute Earth System Model (MPI-ESM) (Jungclaus et al., 2014) (Fig. S4). Most of the precipitation occurs in June–August in the study area, and the evaporation process is intensified in summer (Lan et al., 2018), so we mainly considered the results of June–July–August (JJA). There is a positive relationship between the TSI, temperature, and evaporation (Fig. S4), indicating that high solar output favors high temperature and intensified evaporation at century timescales in arid Central Asia. Moreover, the effective humidity shows a negative association with evaporation, temperature, and TSI variability (Fig. S4). However, the relationship between precipitation and effective humidity appears to be obscure at the century timescale (Fig. S4). Therefore, the solar forcing has a direct contribution to regulating the humidity in ACA by the Gleissberg century cycle forcing on the temperature and evaporation over the last millennium, although water vapor transported by westerlies and precipitation might be affected by ocean–atmosphere modes.

5.3.3 Linkage to ENSO

ENSO is a mode of variability representing changes in sea-surface temperatures and atmospheric circulation across the equatorial Pacific Ocean (Jiménez-Moreno et al., 2021; Cane, 2005). Paleoclimatic proxies and historical records suggest ENSO has long-term variability in amplitude and frequency on multidecadal to centennial timescales (Yeh and Kirtman, 2007; D'Arrigo et al., 2005; Li et al., 2011; Mann et al., 2000). The amplitude of ENSO variability is the important factor to affect the occurrence of climate extremes over the globe (Mcphaden et al., 2006; Cheng et al., 2008). On the multi-centennial timescale (i.e., MWP to LIA), the HI and ENSO variance (Li et al., 2011) show a similar trend in amplitude changes (Fig. 7d). The amplitudes of HI and ENSO variance both show a distinctly increasing trend during the LIA and maintain a relatively high level from $\sim$ 1650 to 1950 CE (Fig. 7d). This trend suggests that the relatively humid environment and unstable hydroclimate in ACA may be associated with the increase in ENSO variance amplitude (Li et al., 2011) and more frequent ENSO events (Rustic et al., 2015) during the LIA, which are possible owing to a major reorganization within the tropical ocean–atmosphere system or significant ENSO teleconnection changes from the MWP to LIA (Rustic et al., 2015; Li et al., 2011). The results here support previous studies showing that ENSO might affect hydroclimate variability in ACA at multi-centennial timescales with La Niña-like (EI Niño-like) conditions during the MWP (LIA) (F. Chen et al., 2019; Chen et al., 2015). During the LIA with relatively warm EI Niño-like conditions, the Western Pacific Subtropical High enhanced and extended westwards, and a low-pressure trough related to the weakening of the Siberian High over the central–southwest Asia region formed, together resulting wetter climatic conditions in arid Central Asia (Chen et al., 2015; F. Chen et al., 2019a; Feng et al., 2016; Syed et al., 2006).

On the multidecadal timescales, however, the WTC between the HI and ENSO variance shows a robust negative phase relationship (Fig. 7e). In particular, the WTC result shows that the HI has a similar quasi-regular cycle of ENSO variance from 82–90 years during the MWP to 50–60 years thereafter (Li et al., 2011), which reveals the potential modulation of these quasi-regular cycles of ENSO variance to extreme humidity oscillations at the multidecadal timescales in ACA (Fig. 7e). Furthermore, the multidecadal component of the HI extracted by the EEMD (Wu and Huang, 2009; Huang et al., 1998) also exhibits an obvious inverse relationship with ENSO variance (Fig. 7g). The influence of ENSO on the extratropical climate has been shown to be modulated by ENSO variance at multidecadal timescales, and the calculated 31-year running correlations between the reconstructed ENSO variance and other records of ENSO teleconnections shows that the ENSO teleconnection is robust over Central Asia during the past seven centuries only except for the Maunder minimum (Li et al., 2013). The quasi-regular

periodic variation of ENSO variance effects on the hydroclimate changes of ACA at multidecadal timescales might be through modulating the extreme precipitation. The water vapor from the Arabian Sea may be transported to the Xinjiang region and cause heavy precipitation, although the water vapor fluxes mostly come from the west transported by the prevailing westerlies (Huang et al., 2015a, 2013). Daily observational precipitation and National Center for Environmental Prediction (NCEP) reanalysis data also suggest that the low-level water vapor fluxes from the Indian Ocean, transported along the eastern periphery of the Tibetan Plateau, are the most important factor leading to rainstorms in ACA (Huang et al., 2017). However, our knowledge of the cause of ENSO variance influence on hydroclimate oscillations in ACA at multidecadal timescales is still in its infancy and remains uncertain, owing to the complicated interactions of the tropical and subtropical ocean basins at decadal to multidecadal timescales (Cai et al., 2019). The mechanisms for the different timescales between the ENSO amplitude and hydroclimate changes in ACA require further exploration through high-resolution records and simulation experiments.

6 Conclusions

We present the humidity index (HI) in ACA over the past millennium based on the $\sim$ 1.8-year high-resolution multiproxy records from Lake Dalongchi in the central Tian Shan. Our results reveal dramatic and unstable multidecadal to century-scale humidity oscillations over the last millennium, especially within the LIA, which is distinct from other records of ACA. Our findings emphasize that the Gleissberg solar cycle and quasi-regular period of ENSO amplitude play critical roles in controlling the effective humidity in ACA at century and multidecadal timescales, respectively. However, high-resolution records on different timescales and climate model simulations are still needed to improve our understanding of the physical mechanisms of the links between solar irradiance and ocean–atmosphere modes and how their coupling affects moisture variation in ACA.

Data availability. The reconstructed humidity index in this study has been submitted to the datasets of the 4TU Center for Research Data, which can will be permanently available at https://doi.org/10.4121/16570398 (Feng et al., 2022).

Supplement. The supplement related to the article contains the supplementary methods and four supplementary diagrams. The supplement related to this article is available online at: https://doi.org/10.5194/cp-18-975-2022-supplement.

Author contributions. SF and XL conceived this study, carried out the laboratory analysis and data interpretation, and wrote the paper. FS and YL performed the data analysis. XM and JW participated in the retrieval of the sediment core and sampling. All authors discussed the results and commented on the paper.

Competing interests. The contact author has declared that neither they nor their co-authors have any competing interests.

Disclaimer. Publisher's note: Copernicus Publications remains neutral with regard to jurisdictional claims in published maps and institutional affiliations.

Acknowledgements. We are grateful to the three anonymous reviewers and editor Mary Gagen for their insightful comments and constructive suggestions, which helped to improve the manuscript. We thank Junfeng Li, Weihan Jia, Huashu Li, Huihui Qi, and Qi Zhang for their help with the field work.

Financial support. This research has been supported by the National Key Research and Development Program of China (grant no. 2018YFA0606400), the National Natural Science Foundation of China (grant no. 41907375), and the Basic Research Program of the Institute of Hydrogeology and Environmental Geology CAGS (grant no. SK202007).

Review statement. This paper was edited by Mary Gagen and reviewed by three anonymous referees.

References

Aichner, B., Feakins, S. J., Lee, J. E., Herzschuh, U., and Liu, X.: High-resolution leaf wax carbon and hydrogen isotopic record of the late Holocene paleoclimate in arid Central Asia, Clim. Past, 11, 619–633, https://doi.org/10.5194/cp-11-619-2015, 2015.

Aizen, E. M., Aizen, V. B., Melack, J. M., Nakamura, T., and Ohta, T.: Precipitation and atmospheric circulation patterns at mid-latitudes of Asia, Int. J. Climatol., 21, 535–556, https://doi.org/10.1002/joc.626, 2001.

Bard, E. and Frank, M.: Climate change and solar variability: What's new under the sun?, Earth Planet. Sci. Lett., 248, 1–14, https://doi.org/10.1016/j.epsl.2006.06.016, 2006.

Bard, E., Raisbeck, G., Yiou, F., and Jouzel, J.: Solar irradiance during the last 1200 years based on cosmogenic nuclides, Tellus B, 52, 985–992, https://doi.org/10.1034/j.1600-0889.2000.d01-7.x, 2000.

Blaauw, M. and Christen, J. A.: Flexible paleoclimate age-depth models using an autoregressive gamma process, Bayesian Anal., 6, 457–474, https://doi.org/10.1214/ba/1339616472, 2011.

Bond, G., Kromer, B., Beer, J., Muscheler, R., Evans, M. N., Showers, W., Hoffmann, S., Lotti-Bond, R., Hajdas, I., and Bonani, G.: Persistent Solar Influence on North Atlantic Climate During the Holocene, Science, 294, 2130–2136, 2001.

Boroninaa, A., Renarda, P., Balderera, W., and Christodoulides, A.: Groundwater resources in the Kouris catchment (Cyprus):

data analysis and numerical modelling, J. Hydrol., 271, 130–149, https://doi.org/10.1016/S0022-1694(02)00322-0, 2003.

Brahim, Y. A., Wassenburg, J. A., Cruz, F. W., Sifedine, A., Scholz, D., Boumchou, L., Dassie, E. P., Jochum, K. P., Edwards, R. L., and Cheng, H.: Multi-decadal to centennial hydroclimate variability and linkage to solar forcing in the Western Mediteraanean during the last 1000 years, Sci. Rep., 8, 1–8, 2018.

Cai, W., Wu, L., Lengaigne, M., Li, T., McGregor, S., Kug, J. S., Yu, J. Y., Stuecker, M. F., Santoso, A., Li, X., Ham, Y. G., Chikamoto, Y., Ng, B., McPhaden, M. J., Du, Y., Dommenget, D., Jia, F., Kajtar, J. B., Keenlyside, N., Lin, X., Luo, J. J., Martin-Rey, M., Ruprich-Robert, Y., Wang, G., Xie, S. P., Yang, Y., Kang, S. M., Choi, J. Y., Gan, B., Kim, G. I., Kim, C. E., Kim, S., Kim, J. H., and Chang, P.: Pantropical climate interactions, Science, 363, 1–11, https://doi.org/10.1126/science.aav4236, 2019.

Cane, M. A.: The evolution of El Niño, past and future, Earth Planet. Sci. Lett., 230, 227–240, https://doi.org/10.1016/j.epsl.2004.12.003, 2005.

Carlson, A. E. and Clark, P. U.: Ice sheet sources of sea level rise and freshwater discharge during the last deglaciation, Rev. Geophys., 50, 1–72, https://doi.org/10.1029/2011rg000371, 2012.

Chen, F., Huang, X., Zhang, J., Holmes, J. A., and Chen, J.: Humid Little Ice Age in arid central Asia documented by Bosten Lake, Xinjiang, China, Sci. China Ser. D, 49, 1280–1290, https://doi.org/10.1007/s11430-006-2027-4, 2006.

Chen, F., Chen, J., Holmes, J., Boomer, I., Austin, P., Gates, J. B., Wang, N., Brooks, S. J., and Zhang, J.: Moisture changes over the last millennium in arid central Asia: a review, synthesis and comparison with monsoon region, Quaternary Sci. Rev., 29, 1055–1068, https://doi.org/10.1016/j.quascirev.2010.01.005, 2010.

Chen, F., Jia, J., Chen, J., Li, G., Zhang, X., Xie, H., Xia, D., Huang, W., and An, C.: A persistent Holocene wetting trend in arid central Asia, with wettest conditions in the late Holocene, revealed by multi-proxy analyses of loess-paleosol sequences in Xinjiang, China, Quaternary Sci. Rev., 146, 134–146, https://doi.org/10.1016/j.quascirev.2016.06.002, 2016.

Chen, F., Chen, J., Huang, W., Chen, S., Huang, X., Jin, L., Jia, J., Zhang, X., An, C., Zhang, J., Zhao, Y., Yu, Z., Zhang, R., Liu, J., Zhou, A., and Feng, S.: Westerlies Asia and monsoonal Asia: Spatiotemporal differences in climate change and possible mechanisms on decadal to sub-orbital timescales, Earth Sci. Rev., 192, 337–354, https://doi.org/10.1016/j.earscirev.2019.03.005, 2019a.

Chen, J., Chen, F., Feng, S., Huang, W., Liu, J., and Zhou, A.: Hydroclimatic changes in China and surroundings during the Medieval Climate Anomaly and Little Ice Age: spatial patterns and possible mechanisms, Quaternary Sci. Rev., 107, 98–111, https://doi.org/10.1016/j.quascirev.2014.10.012, 2015.

Chen, J., Chen, F., Zhang, E., Brooks, S. J., Zhou, A., and Zhang, J.: A 1000-year chironomid-based salinity reconstruction from varved sediments of Sugan Lake, Qaidam Basin, arid Northwest China, and its palaeoclimatic significance, Chi. Sci. Bull., 54, 3749–3759, https://doi.org/10.1007/s11434-009-0201-8, 2009.

Chen, J., Liu, J., Zhang, X., Chen, S., Huang, W., Chen, J., Zhang, S., Zhou, A., and Chen, F.: Unstable Little Ice Age climate revealed by high-resolution proxy records from northwestern China, Clim. Dynam., 53, 1–10, https://doi.org/10.1007/s00382-019-04685-5, 2019b.

Cheng, Y., Zhou, X., Deng, Z., Tang, Y., and Chen, D.: Interdecadal Variation of ENSO Predictability in Multiple Models, J. Climate, 21, 4811–4833, https://doi.org/10.1175/2008jcli2193.1, 2008.

D'Arrigo, R., Cook, E. R., Wilson, R. J., Allan, R., and Mann, M. E.: On the variability of ENSO over the past six centuries, Geophys. Res. Lett., 32, L03711, https://doi.org/10.1029/2004GL022055., 2005.

Feng, Z., Sun, A., Abdusalih, N., Ran, M., Kurban, A., Lan, B., Zhang, D., and Yang, Y.: Vegetation changes and associated climatic changes in the southern Altai Mountains within China during the Holocene, The Holocene, 27, 683–693, https://doi.org/10.1177/0959683616670469, 2016.

Feng, S., Liu, X., Shi, F., Mao, X., Li, Y., and Wang, J.: Supplementary data for Humidity changes and possible forcing mechanisms over the last millennium in arid Central Asia, 4TU Research Data [data set], https://doi.org/10.4121/16570398, 2022.

Gao, J., Li, M., Xiao, X., Tang, Y., and He, G.: Paleozoic tectonic evolution of the Tianshan Orogen, northwestern China, Tectonophysics, 287, 213–231, https://doi.org/10.1016/S0040-1951(98)80070-X, 1998.

Gates, J. B., Edmunds, W. M., Ma, J., and Sheppard, P. R.: A 700-year history of groundwater recharge in the drylands of NW China, The Holocene, 18, 1045–1054, https://doi.org/10.1177/0959683608095575, 2008.

Gimeno, L., Torre, L. d. L., Nieto, R., Garcia, R., Hernandez, E., and Ribera, P.: Changes in the relationship NAO Northern hemisphere temperature due to solar activity, Earth Planet. Sci. Lett., 203, 15–20, https://doi.org/10.1016/S0012-821X(02)01090-7, 2003.

Gleissberg, W.: The eighty-year sunspot cycle, J. Br. Astron. Assoc., 68, 148–152, 1958.

Gleissberg, W.: The eighty-year sunspot cycle in auroral frequency numbers, J. Br. Astron. Assoc., 75, 227–231, 1965.

Gray, L. J.: The influence of the equatorial upper stratosphere on stratospheric sudden warmings, Geophys. Res. Lett., 30, 4, https://doi.org/10.1029/2002gl016430, 2003.

Grinsted, A., Moore, J. C., and Jevrejeva, S.: Application of the cross wavelet transform and wavelet coherence to geophysical time series, Nonlin. Processes Geophys., 11, 561–566, https://doi.org/10.5194/npg-11-561-2004, 2004.

He, Y., Zhao, C., Wang, Z., Wang, H., Song, M., Liu, W., and Liu, Z.: Late Holocene coupled moisture and temperature changes on the northern Tibetan Plateau, Quaternary Sci. Rev., 80, 47–57, https://doi.org/10.1016/j.quascirev.2013.08.017, 2013.

Huang, N. E., Shen, Z., Long, S. R., Wu, M. C., Shih, H. H., Zheng, Q., Yen, N.-C., Tong, C. C., and Liu, H. H.: The empirical mode decomposition and the Hilbert spectrum for nonlinear and non-stationary time series analysis, Proc. Roy. Soc. London, 454, 903–995, https://doi.org/10.1098/rspa.1998.0193, 1998.

Huang, W., Chen, F., Feng, S., Chen, J., and Zhang, X.: Interannual precipitation variations in the mid-latitude Asia and their association with large-scale atmospheric circulation, Chi. Sci. Bull., 58, 3962–3968, https://doi.org/10.1007/s11434-013-5970-4, 2013.

Huang, W., Feng, S., Chen, J., and Chen, F.: Physical Mechanisms of Summer Precipitation Variations in the Tarim Basin in Northwestern China, J. Climate, 28, 3579–3591, https://doi.org/10.1175/jcli-d-14-00395.1, 2015a.

Huang, W., Chen, J., Zhang, X., Feng, S., and Chen, F.: Definition of the core zone of the "westerlies-dominated climatic regime",

and its controlling factors during the instrumental period, Sci. Chi. Earth Sci., 58, 676–684, https://doi.org/10.1007/s11430-015-5057-y, 2015b.

Huang, W., Chang, S.-Q., Xie, C.-L., and Zhang, Z.-P.: Moisture sources of extreme summer precipitation events in North Xinjiang and their relationship with atmospheric circulation, Adv. Clim. Change Res., 8, 12–17, https://doi.org/10.1016/j.accre.2017.02.001, 2017.

Huang, X., Oberhänsli, H., von Suchodoletz, H., Prasad, S., Sorrel, P., Plessen, B., Mathis, M., and Usubaliev, R.: Hydrological changes in western Central Asia (Kyrgyzstan) during the Holocene as inferred from a palaeolimnological study in lake Son Kul, Quaternary Sci. Rev., 103, 134–152, https://doi.org/10.1016/j.quascirev.2014.09.012, 2014.

Hurrell, J. W.: Decadal trends in the north atlantic oscillation: regional temperatures and precipitation, Science, 269, 676–679, https://doi.org/10.1126/science.269.5224.676, 1995.

Ineson, S., Scaife, A. A., Knight, J. R., Manners, J. C., Dunstone, N. J., Gray, L. J., and Haigh, J. D.: Solar forcing of winter climate variability in the Northern Hemisphere, Nat. Geosci., 4, 753–757, https://doi.org/10.1038/NGEO1282, 2011.

Jeanpert, J., Iseppi, M., Adler, P. M., Genthon, P., Sevin, B., Thovert, J. F., Dewandel, B., and Join, J. L.: Fracture controlled permeability of ultramafic basement aquifers. Inferences from the Koniambo massif, New Caledonia, Eng. Geol., 256, 67–83, https://doi.org/10.1016/j.enggeo.2019.05.006, 2019.

Jiménez-Moreno, G., Anderson, R. S., and Shinker, J. J.: ENSO, sun and megadroughts in SW USA during the last 11,000 years, Earth Planet. Sci. Lett., 576, 117217, https://doi.org/10.1016/j.epsl.2021.117217, 2021.

Jin, L., Chen, F., Morrill, C., Otto-Bliesner, B. L., and Rosenbloom, N.: Causes of early Holocene desertification in arid central Asia, Clim. Dynam., 38, 1577–1591, https://doi.org/10.1007/s00382-011-1086-1, 2011.

Jungclaus, J. H., Lohmann, K., and Zanchettin, D.: Enhanced 20th-century heat transfer to the Arctic simulated in the context of climate variations over the last millennium, Clim. Past, 10, 2201–2213, https://doi.org/10.5194/cp-10-2201-2014, 2014.

Kirov, B. and Georgieva, K.: Long-term variations and interrelations of ENSO, NAO and solar activity, Phys. Chem. Earth, 27, 441–448, https://doi.org/10.1016/S1474-7065(02)00024-4, 2002.

Knudsen, M. F., Jacobsen, B. H., Seidenkrantz, M. S., and Olsen, J.: Evidence for external forcing of the Atlantic Multidecadal Oscillation since termination of the Little Ice Age, Nat. Commun., 5, 3323, https://doi.org/10.1038/ncomms4323, 2014.

Kodera, K.: Solar cycle modulation of the North Atlantic Oscillation: Implication in the spatial structure of the NAO, Geophys. Res. Lett., 29, 59-51–59-54, https://doi.org/10.1029/2001gl014557, 2002.

Kodera, K. and Kuroda, Y.: Dynamical response to the solar cycle, J. Geophys. Res.-Atmos., 107, 4749, https://doi.org/10.1029/2002jd002224, 2002.

Lan, J., Xu, H., Sheng, E., Yu, K., Wu, H., Zhou, K., Yan, D., Ye, Y., and Wang, T.: Climate changes reconstructed from a glacial lake in High Central Asia over the past two millennia, Quaternary Int., 487, 43–53, https://doi.org/10.1016/j.quaint.2017.10.035, 2018.

Lan, J., Xu, H., Yu, K., Sheng, E., Zhou, K., Wang, T., Ye, Y., Yan, D., Wu, H., Cheng, P., Abuliezi, W., and Tan,L.: Late Holocene hydroclimatic variations and possible forcing mechanisms over the eastern Central Asia, Sci. China, 62, 1288-1301, https://doi.org/10.1007/s11430-018-9240-x, 2019.

Lauterbach, S., Witt, R., Plessen, B., Dulski, P., Prasad, S., Mingram, J., Gleixner, G., Hettler-Riedel, S., Stebich, M., Schnetger, B., Schwalb, A., and Schwarz, A.: Climatic imprint of the mid-latitude Westerlies in the Central Tian Shan of Kyrgyzstan and teleconnections to North Atlantic climate variability during the last 6000 years, The Holocene, 24, 970–984, https://doi.org/10.1177/0959683614534741, 2014.

Lei, Y., Tian, L., Bird, B. W., Hou, J., Ding, L., Oimahmadov, L., and Gadoev, M.: A 2540-year record of moisture variations derived from lacustrine sediment (Sasikul Lake) on the Pamir Plateau, The Holocene, 2014, 1–10, https://doi.org/10.1177/0959683614530443, 2014.

Li, J., Xie, S.-P., Cook, E. R., Huang, G., D'Arrigo, R., Liu, F., Ma, J., and Zheng, X.-T.: Interdecadal modulation of El Niño amplitude during the past millennium, Nat. Clim. Change, 1, 114–118, https://doi.org/10.1038/NCLIMATE1086, 2011.

Li, J., Xie, S.-P., Cook, E. R., Morales, M. S., Christie, D. A., Johnson, N. C., Chen, F., D'Arrigo, R., Fowler, A. M., Gou, X., and Fang, K.: El Niño modulations over the past seven centuries, Nat. Clim. Change, 3, 822–826, https://doi.org/10.1038/nclimate1936, 2013.

Li, Z., Chen, Y., Wang, Y., and Li, W.: Drought promoted the disappearance of civilizations along the ancient Silk Road, Environ. Earth Sci., 75, 1116, https://doi.org/10.1007/s12665-016-5925-6, 2016.

Ling, Y., Dai, X., Zheng, M., Sun, Q., Chu, G., Wang, H., Xie, M., and Shan, Y.: High-resolution geochemical record for the last 1100 yr from Lake Toson, northeastern Tibetan Plateau, and its climatic implications, Quaternary Int., 487, 61–70, https://doi.org/10.1016/j.quaint.2017.03.067, 2018.

Liu, X., Rao, Z., Shen, C. C., Liu, J., Chen, J., Chen, S., Wang, X., and Chen, F.: Holocene Solar Activity Imprint on Centennial- to Multidecadal-Scale Hydroclimatic Oscillations in Arid Central Asia, J. Geophys. Res.-Atmos., 124, 2562–2573, https://doi.org/10.1029/2018jd029699, 2019.

Lods, G., Roubinet, D., Matter, J. M., Leprovost, R., and Gouze, P.: Groundwater flow characterization of an ophiolitic hard-rock aquifer from cross-borehole multilevel hydraulic experiments, J. Hydrol., 589, 125152, https://doi.org/10.1016/j.jhydrol.2020.125152, 2020.

Ma, C., Wang, F., Cao, Q., Xia, X., Li, S., and Li, X.: Climate and environment reconstruction during the Medieval Warm Period in Lop Nur of Xinjiang, China, Sci. Bull., 53, 3016–3027, https://doi.org/10.1007/s11434-008-0366-6, 2008.

Ma, J. and Edmunds, W. M.: Groundwater and lake evolution in the Badain Jaran Desert ecosystem, Inner Mongolia, Hydrogeol. J., 14, 1231–1243, https://doi.org/10.1007/s10040-006-0045-0, 2006.

Ma, Z., Xia, L., Xu, X., Xia, Z., Li, X., and Wang, L.: Geochemical characteristics of basalts: evidence for the tectonic setting and geological significance of Kulehu ophiolite, South Tianshan Mountains, Acta Petrol. Mineral., 25, 387–400, https://doi.org/10.1016/S1872-2040(06)60043-1, 2006 (in Chinese with English Abstruct).

Mahaney, W. C., Dirszowsky, R. W., Milner, M. W., Menzies, J., Stewart, A., Kalm, V., and Bezada, M.: Quartz microtextures and

microstructures owing to deformation of glaciolacustrine sediments in the northern Venezuelan Andes, J. Quaternary Sci., 19, 23–33, https://doi.org/10.1002/jqs.818, 2004.

Mann, M. E., Bradley, R. S., and Hughes, M. K.: Long-term variability in the El Niño/Southern Oscillation and associated teleconnections, in: ENSO: Multiscale Variability and Global and Regional Impacts, edited by: Diaz, H. F. and Markgraf, V., Cambridge University Press, Cambridge, 357–412, 2000.

Mathis, M., Sorrel, P., Klotz, S., Huang, X., and Oberhänsli, H.: Regional vegetation patterns at lake Son Kul reveal Holocene climatic variability in central Tien Shan (Kyrgyzstan, Central Asia), Quaternary Sci. Rev., 89, 169–185, https://doi.org/10.1016/j.quascirev.2014.01.023, 2014.

McPhaden, M. J., Zebiak, S. E., and Glantz, M. H.: ENSO as an integrating concept in Earth science, Science, 314, 1740–1745, 2006.

Meyers, P. A.: Preservation of elemental and isotopic source identification of sedimentary organic matter, Chem. Geol., 114, 289–302, https://doi.org/10.1016/0009-2541(94)90059-0, 1994.

Meyers, P. A.: Applications of organic geochemistry to paleolimnological reconstructions: a summary of examples from the Laurentian Great Lakes, Organ. Geochem., 34, 261–289, https://doi.org/10.1016/S0146-6380(02)00168-7, 2003.

Moffa-Sánchez, P., Born, A., Hall, I. R., Thornalley, D. J. R., and Barker, S.: Solar forcing of North Atlantic surface temperature and salinity over the past millennium, Nat. Geosci., 7, 275–278, https://doi.org/10.1038/NGEO2094, 2014.

Moral Cardona, J. P., Gutiérrez Mas, J. M., Sánchez Bellón, A., Domínguez-Bella, S., and Martínez López, J.: Surface textures of heavy-mineral grains: a new contribution to provenance studies, Sediment. Geol., 174, 223–235, https://doi.org/10.1016/j.sedgeo.2004.12.006, 2005.

Narisma, G. T., Foley, J. A., Licker, R., and Ramankutty, N.: Abrupt changes in rainfall during the twentieth century., Geophys. Res. Lett., 34, 306–316, https://doi.org/10.1029/2006GL028628, 2007.

Ogurtsov, M., Lindholm, M., Jalkanen, R., and Veretenenko, S.: Evidence for the Gleissberg solar cycle at the high-latitudes of the Northern Hemisphere, Adv. Space Res., 55, 1285–1290, https://doi.org/10.1016/j.asr.2014.11.031, 2015.

Ogurtsov, M. G., Nagovitsyn, Y. A., Kocharov, G. E., and Jungner, H.: Long-Period Cycles of the Sun's Activity Recorded in Direct Solar Data and Proxies, Solar Phys., 211, 371–394, https://doi.org/10.1023/A:1022411209257, 2002a.

Ogurtsov, M. G., Kocharov, G. E., Lindholm, M., Meriläinen, J., Eronen, M., and Nagovitsyn, Y. A.: Evidence of Solar Variation in Tree-Ring-Based Climate Reconstructions, Solar Phys., 205, 403–417, https://doi.org/10.1023/A:1014277121166, 2002b.

Ortega, P., Lehner, F., Swingedouw, D., Masson-Delmotte, V., Raible, C. C., Casado, M., and Yiou, P.: A model-tested North Atlantic Oscillation reconstruction for the past millennium, Nature, 523, 71–74, https://doi.org/10.1038/nature14518, 2015.

Pennington, W., Tutin, T. G., Cambary, R. S., and Fisher, E. M.: Observations on lake sediments using fallout ^{137}Cs as a tracer, Nature, 242, 324–326, https://doi.org/10.1038/242324a0, 1973.

Rousseau, M., Demory, F., Miramont, C., Brisset, E., Guiter, F., Sabatier, P., and Sorrel, P.: Palaeoenvironmental change and glacier fluctuations in the high Tian Shan Mountains during the last millennium based on sediments from Lake Ala Kol, Kyrgyzstan, Palaeogeography, Palaeoclimatology, Palaeoecology, 558, 109987, https://doi.org/10.1016/j.palaeo.2020.109987, 2020.

Rustic, G. T., Koutavas, A., Marchitto, T. M., and Linsley, B. K.: Dynamical excitation of the tropical Pacific Ocean and ENSO variability by Little Ice Age cooling, Science, 350, 1537–1541, https://doi.org/10.1126/science.aac9937, 2015.

Schwarz, A., Turner, F., Lauterbach, S., Plessen, B., Krahn, K. J., Glodniok, S., Mischke, S., Stebich, M., Witt, R., Mingram, J., and Schwalb, A.: Mid- to late Holocene climate-driven regime shifts inferred from diatom, ostracod and stable isotope records from Lake Son Kol (Central Tian Shan, Kyrgyzstan), Quaternary Sci. Rev., 177, 340–356, https://doi.org/10.1016/j.quascirev.2017.10.009, 2017.

Sha, L., Jiang, H., Seidenkrantz, M.-S., Muscheler, R., Zhang, X., Knudsen, M. F., Olsen, J., Knudsen, K. L., and Zhang, W.: Solar forcing as an important trigger for West Greenland sea-ice variability over the last millennium, Quaternary Sci. Rev., 131, 148–156, https://doi.org/10.1016/j.quascirev.2015.11.002, 2016.

Shindell, D. T., Schmidt, G. A., Mann, M. E., Rind, D., and Waple, A.: Solar Forcing of Regional Climate Change During the Maunder Minimum, Science, 294, 2149–2152, https://doi.org/10.1126/science.1064363, 2001.

Song, M., Zhou, A., Zhang, X., Zhao, C., He, Y., Yang, W., Liu, W., Li, S., and Liu, Z.: Solar imprints on Asian inland moisture fluctuations over the last millennium, The Holocene, 5, 1935–1943, https://doi.org/10.1177/0959683615596839, 2015.

Sorrel, P., Jacq, K., Van Exem, A., Escarguel, G., Dietre, B., Debret, M., McGowan, S., Ducept, J., Gauthier, E., and Oberhänsli, H.: Evidence for centennial-scale Mid-Holocene episodes of hypolimnetic anoxia in a high-altitude lake system from central Tian Shan (Kyrgyzstan), Quaternary Sci. Rev., 252, 106748, https://doi.org/10.1016/j.quascirev.2020.106748, 2021.

Swingedouw, D., Terray, L., Cassou, C., Voldoire, A., Salas-Mélia, D., and Servonnat, J.: Natural forcing of climate during the last millennium: fingerprint of solar variability, Clim. Dynam., 36, 1349–1364, https://doi.org/10.1007/s00382-010-0803-5, 2011.

Syed, F. S., Giorgi, F., Pal, J. S., and King, M. P.: Effect of remote forcings on the winter precipitation of central southwest Asia part 1: observations, Theor. Appl. Climatol., 86, 147–160, https://doi.org/10.1007/s00704-005-0217-1, 2006.

Trouet, V., Esper, J., Graham, N. E., Baker, A., Scourse, J. D., and Frank, D. C.: Persistent Positive North Atlantic Oscillation Mode Dominated the Medieval Climate Anomaly, Science, 324, 78–80, https://doi.org/10.1126/science.1166349, 2009.

Wang, J., Yang, B., Ljungqvist, F. C., Luterbacher, J., Osborn, Timothy J., Briffa, K. R., and Zorita, E.: Internal and external forcing of multidecadal Atlantic climate variability over the past 1,200 years, Nat. Geosci., 10, 512–517, https://doi.org/10.1038/NGEO2962, 2017.

Wolff, C., Plessen, B., Dudashvilli, A. S., Breitenbach, S. F. M., Cheng, H., Edwards, L. R., and Strecker, M. R.: Precipitation evolution of Central Asia during the last 5000 years, The Holocene, 27, 142–154, https://doi.org/10.1177/0959683616652711, 2016.

Wu, D., Zhou, A., Zhang, J., Chen, J., Li, G., Wang, Q., Chen, L., Madsen, D., Abbott, M., Cheng, B., and Chen, F.: Temperature-induced dry climate in basins in the northeastern Tibetan Plateau during the early to middle Holocene, Quaternary Sci. Rev., 237, 106311, https://doi.org/10.1016/j.quascirev.2020.106311, 2020.

Wu, Z. and Huang, N. E.: Ensemble Empirical Mode Decomposition: A Noise-Assisted Data Analysis Method, Adv. Adapt. Data Anal., 1, 1–41, 2009.

Xiao, W., Windley, B. F., Allen, M. B., and Han, C.: Paleozoic multiple accretionary and collisional tectonics of the Chinese Tianshan orogenic collage, Gondwana Res., 23, 1316–1341, https://doi.org/10.1016/j.gr.2012.01.012, 2013.

Yan, D., Xu, H., Lan, J., Zhou, K., Ye, Y., Zhang, J., An, Z., and Yeager, K. M.: Solar activity and the westerlies dominate decadal hydroclimatic changes over arid Central Asia, Global Planet. Change, 173, 53–60, https://doi.org/10.1016/j.gloplacha.2018.12.006, 2019.

Yang, B., Wang, J., Bräuning, A., Dong, Z., and Esper, J.: Late Holocene climatic and environmental changes in arid central Asia, Quaternary Int., 194, 68–78, https://doi.org/10.1016/j.quaint.2007.11.020, 2009.

Yeh, S.-W. and Kirtman, B. P.: ENSO amplitude changes due to climate change projections in different coupled models, J. Climate, 20, 203–217, https://doi.org/10.1175/JCLI4001.1, 2007.

Yin, Z.-Y., Zhu, H., Huang, L., and Shao, X.: Reconstruction of biological drought conditions during the past 2847 years in an alpine environment of the northeastern Tibetan Plateau, China, and possible linkages to solar forcing, Global Planet. Change, 143, 214–227, https://doi.org/10.1016/j.gloplacha.2016.04.010, 2016.

Yukimoto, S., Kodera, K., and Thiéblemont, R.: Delayed North Atlantic Response to Solar Forcing of the Stratospheric Polar Vortex, Sola, 13, 53–58, https://doi.org/10.2151/sola.2017-010, 2017.

Zhang, B., Liu, X., and Li, J.: The aeolian component inferred from lake sediments in China, Aeolian Res., 50, 100700, https://doi.org/10.1016/j.aeolia.2021.100700, 2021a.

Zhang, M., Liu, X., Yu, Z., and Wang, Y.: Paleolake evolution in response to climate change since middle MIS 3 inferred from Jilantai Salt Lake in the marginal regions of the ASM domain, Quaternary Int., 607, 48–57, https://doi.org/10.1016/j.quaint.2021.06.017, 2021b.

Zhang, Q.-B., Cheng, G., Yao, T., Kang, X., and Huang, J.: A 2,326-year tree-ring record of climate variability on the northeastern Qinghai-Tibetan Plateau, Geophys. Res. Lett., 30, 14, https://doi.org/10.1029/2003gl017425, 2003.

Zhang, Q., Liu, X., and Li, H.: Impact of hydrological conditions on the radiocarbon reservoir effect in lake sediment 14C dating: the case of Kusai Lake on the northern Qinghai-Tibet Plateau, Quaternary Geochronol., 62, 101149, https://doi.org/10.1016/j.quageo.2020.101149, 2021c.

Zhang, Y., Kong, Z., Yan, S., Yang, Z., and Ni, J.: "Medieval Warm Period" on the northern slope of central Tianshan Mountains, Xinjiang, NW China, Geophys. Res. Lett., 36, 1–5, https://doi.org/10.1029/2009GL037375, 2009.

Zhao, C., Yu, Z., and Ito, E.: Possible orographic and solar controls of Late Holocene centennialscale moisture oscillations in the northeastern Tibetan Plateau, Geophys. Res. Lett., 36, L21705, https://doi.org/10.1029/2009GL040951, 2009.

Zhou, J., Wang, X., and Niu, R.: Climate characteristics of sandstorm in China in recent 47 years, J. Appl. Meteorol. Sci., 13, 195–200, 2002 (in Chinese with English Abstruct).